Highlights from the k_T-factorization approach on the quarkonium production puzzles

S. P. Baranov*
P. N. Lebedev Institute of Physics, Leninsky prosp. 53, Moscow 117924, Russia
(Received 15 October 2001; published 18 December 2002)

In the framework of the k_T-factorization approach, we analyze the production of various quarkonium states at modern colliders and discuss the origin and the size of theoretical uncertainties. We find that the effects of the initial gluon off-shellness can provide a reasonable explanation for the J/ψ spin alignment in both pp and ep collisions. We point out the fundamental role of the polarization observables, which indicate a clear difference between the collinear and noncollinear interpretations of QCD.

DOI: 10.1103/PhysRevD.66.114003 PACS number(s): 12.38.Bx, 13.85.Ni, 14.40.Gx

I. INTRODUCTION

At the energies of modern colliders, the interaction dynamics is governed by the properties of parton distributions in the small x region. This domain is characterized by the double inequality $s \gg \mu^2 \simeq \hat{s} \gg \Lambda^2$, which shows that the typical parton interaction scale μ (of the order of the subprocess invariant energy $\sqrt{\hat{s}}$) is much higher than the QCD parameter Λ, but is much lower than the total c.m. system energy $\sqrt{s}$. The situation is therefore classified as ''semihard.'' In such a case, the perturbation expansion in α_s may contain large coefficients $O[\ln(s/\mu^2)] = O[\ln(1/x)]$ which compensate the smallness of the coupling constant $\alpha_s(\mu^2/\Lambda^2)$. The resummation [1–4] of the terms $[\ln(\mu^2/\Lambda^2)\alpha_s]^n$, $[\ln(\mu^2/\Lambda^2)\ln(1/x)\alpha_s]^n$, and $[\ln(1/x)\alpha_s]^n$ results in the so called noncollinear or unintegrated parton distributions $\mathcal{F}_i(x,k_T^2,\mu^2)$, which determine the probability of finding a parton of type i carrying the longitudinal momentum fraction x and transverse momentum k_T at the probing scale μ^2. These k_T-dependent distributions generalize the factorization of the hadronic matrix elements beyond the collinear approximation. Hereafter this generalized factorization will be referred to as ''k_T factorization.'' The unintegrated parton distributions obey certain evolution equations [e.g., Balitskiĭ-Fadin-Kuraev-Lipatov (BFKL) [5] or Ciafaloni, Catani, Fiorani, Marchesini (CCFM) [6]] and reduce to conventional Dokshitzer-Gribov-Lipatov-Altarelli-Parisi (DGLAP) [7] densities once the k_T dependence is integrated out.

Nowadays, the significance of the k_T-factorization (semihard) approach is becoming more and more commonly recognized. Its applications to a variety of photo-, lepto-, and hadroproduction processes are widely discussed in the literature [8–12]. Remarkable agreement is found between the data and the theoretical calculations regarding the photo- [13] and electroproduction [14] of D^* mesons and forward jets [15], as well as for specific kinematic correlations observed in the associated D^*+jets photoproduction [16] at the DESY ep collider HERA. The semihard approach was also shown to reasonably describe the data on the hadroproduction of beauty [17,18], J/ψ [19], and $\chi_c$mesons [20] at the Fermilab Tevatron. The theoretical predictions made in Ref. [21] have triggered dedicated experimental analyses [22,23] of the J/ψ polarization (i.e., spin alignment) at HERA conditions.

The problem of J/ψ polarization at ep and pp colliders is an intriguing subject in modern physics. The puzzling history of J/ψ traces back to the early 1990s, when the data [24–27] on the J/ψ and Υ hadroproduction cross sections revealed a more than one order of magnitude discrepancy with theoretical expectations [28,29]. This fact has induced extensive theoretical activity. In particular, it led to the introduction of a new production mechanism, the so called color-octet model [30–38]. Since then, the color-octet model has been believed to give the most likely explanation of the quarkonium production phenomena, although there are also some indications that it is not working well. One of the problems is connected to the photoproduction data [39,40] where the contribution from the color-octet mechanism is unnecessary or even unwanted [41–43] as the experimental results can be described within the color-singlet model alone [44]. Another difficulty refers to the J/ψ spin alignment. If, as expected, the dominant contribution comes from the gluon fragmentation into an octet $c\bar{c}$ pair, the mesons must have strong transverse polarization [43–47]. This is in disagreement with the data [48,49], which point to unpolarized or even longitudinally polarized mesons.

Several attempts have been made in the literature to incorporate the color-octet model within the k_T-factorization approach [50,51]. Some interesting results have been obtained, although still failing to offer a consistent solution of the polarization problem. In this paper, we reconsider the overall situation regarding the production of quarkonium states (including both charm and beauty families, both pp and ep collisions, with respect to both p_T spectra and polarization properties) and present our understanding of the matter. The outline of the paper is the following. In Sec. II we briefly recall the basic principles of the color-singlet and color-octet models and explain their extensions to the k_T-factorization approach. The necessary technical details are described in Sec. III. The numerical results followed by a

*Email address: baranov@sci.lebedev.ru

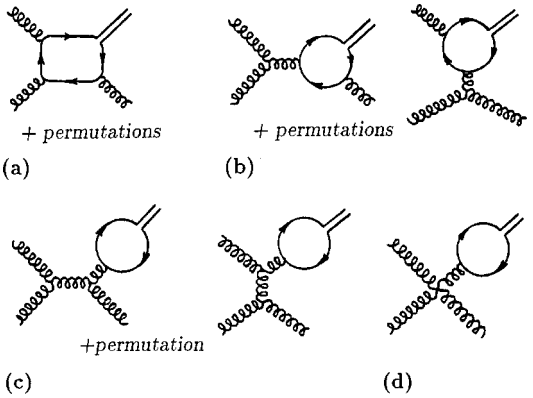

FIG. 1. Feynman diagrams representing the gluon-gluon fusion mechanism in the color-singlet and color-octet models. Only the perturbative skeleton of the process is presented; the soft gluons corresponding to the nonperturbative color-octet transitions are not shown.

discussion are presented in Sec. IV. Finally, the conclusions are formulated in Sec. V.

II. THE MODEL

In the framework of the color-singlet approach [28,29], the production of any heavy meson is described as the perturbative production of a color-singlet $Q\overline{Q}$ pair with the quantum numbers of the quarkonium state under consideration. The corresponding Feynman diagrams are shown in Fig. 1(a) (assuming also five possible permutations of the incoming and outgoing gluons). The formation of a meson from the quark pair is a nonperturbative process. Within the nonrelativistic approximation which we are using, this probability reduces to a single parameter related to the meson wave function at the origin $|\mathcal{R}(0)|^2$, which is known for the J/ψ and Υ families from the measured leptonic decay widths.

In addition to the above, we consider the color-octet production scheme [30–33], which implies that the heavy $Q\overline{Q}$ pair is perturbatively created in a hard subprocess as an octet color state and subsequently evolves into a physical quarkonium state via emitting soft (nonperturbative) gluons, which may be interpreted as a series of ''classical'' color-dipole transitions. Although these transition probabilities can, in principle, be expressed in terms of field operators and therefore calculated, no such calculation exists to date. Thus, the transition probabilities remain free parameters, which are assumed to obey a definite hierarchy in powers of v, the relative velocity of the quarks in the bound system under study. This freedom is commonly used to estimate the color-octet parameters by adjusting them to experimental data. In the case when the color-octet $Q\overline{Q}$ state is allowed, there appear additional contributions due to the diagrams shown in Figs. 1(b)–1(d). The complete gauge invariant set comprises six diagrams of the type (a), six diagrams of the type (b), four diagrams of the type (c), and one diagram (d).

The nonperturbative transition matrix elements mentioned here (usually denoted in the literature as $\langle 0|\mathcal{O}_8|0\rangle$) are related to the fictituous color-octet wave functions, which are used in calculations in place of the ordinary color-singlet wave functions:

$$\langle 0|\mathcal{O}_8|0\rangle=\frac{9}{2\pi}|\mathcal{R}_8(0)|^2=\frac{9}{2\pi}4\pi|\Psi_8(0)|^2.$$

This equation applies to all S-wave color-octet states, and a similar relation holds for $\mathcal{R}'_8(0)$ and $\Psi'_8(0)$ if the P-wave color-octet states are involved. For the sake of uniformity, we will be consistently using the notation in terms of $\mathcal{R}(0)$ and $\mathcal{R}'(0)$ for both color-singlet and color-octet contributions.

A generalization of the above formalism to the k_T-factorization approach implies two important steps. These are the introduction of noncollinear gluon distributions and the modification of the gluon spin density matrix in the parton level matrix elements.

To understand the basic features of k_T factorization, it is useful to rely upon the analogy between QCD and QED. In electrodynamics, one has the well-known Weizsäcker-Williams approximation (WWA), which essentially plays the role of the collinear parton model. In this approach, the ''parton'' photons are assumed to be on mass shell, and their transverse momentum is neglected. On the other hand, a more accurate formula [known as the equivalent photon approximation (EPA)] presents an explicit dependence on the photon virtuality k^2, and there exists a kinematic connection between the virtuality and the photon transverse momentum k_T: $k^2=k_T^2/(1-x)$, where x is the photon longitudinal momentum fraction. The step that is made in QED when passing from the WWA to the EPA is now repeated in QCD. In k_T factorization, one takes into account that gluons generated in the parton evolution cascade do carry non-negligible transverse momentum and are off mass shell.

In the equivalent photon approximation, the off-shell photon spin density matrix is given by the full lepton tensor

$$\overline{\epsilon^\mu\epsilon^{*\nu}}\sim L^{\mu\nu}=8p^\mu p^\nu-4(pk)g^{\mu\nu}, \tag{1}$$

where p is the momentum of the beam particle, and k the momentum of the emitted photon. A similar anzatz [Eq. (2), see below] is used in the k_T-factorization approach. Neglecting the second term in the right hand side of Eq. (1) in the small x limit, $p\gg k$, one arrives at the spin structure $\overline{\epsilon^\mu\epsilon^{*\nu}}\sim p^\mu p^\nu$. The latter can be rewritten in the form

$$\overline{\epsilon^\mu\epsilon^{*\nu}}=k_T^\mu k_T^\nu/|k_T|^2, \tag{2}$$

where we have represented the four-momentum k as $k=xp+k_T$ and applied a gauge shift $\epsilon^\mu\to\epsilon^\mu-k^\mu/x$. This formula converges to the usual $\Sigma\epsilon^\mu\epsilon^{*\nu}=-g^{\mu\nu}$ when $k_T\to 0$. As we will see in Sec. IV, the presence of longitudinal components in the off-shell gluon spin density matrix has an important impact on the quarkonium polarization properties.

In the numerical analysis, we have tried four different sets of k_T-dependent gluon densities. In the approach of Ref. [52] based on a leading-order perturbative solution of the BFKL equation, the unintegrated gluon density $\mathcal{F}_g(x,k_T^2,\mu^2)$ is cal-

culated as a convolution of the ordinary (collinear) gluon density $G(x,\mu^2)$ with universal weight factors:

$$\mathcal{F}_g(x,k_T^2,\mu^2)=\int_x^1 \mathcal{G}(\eta,k_T^2,\mu^2)\frac{x}{\eta}G\left(\frac{x}{\eta},\mu^2\right)d\eta, \tag{3}$$

$$\mathcal{G}(\eta,k_T^2,\mu^2)=\frac{\bar{\alpha}_s}{\eta k_T^2}J_0(2\sqrt{\bar{\alpha}_s\ln(1/\eta)\ln(\mu^2/k_T^2)}),$$

$$k_T^2<\mu^2, \tag{4}$$

$$\mathcal{G}(\eta,k_T^2,\mu^2)=\frac{\bar{\alpha}_s}{\eta k_T^2}I_0(2\sqrt{\bar{\alpha}_s\ln(1/\eta)\ln(k_T^2/\mu^2)}),$$

$$k_T^2>\mu^2, \tag{5}$$

where J_0 and I_0 stand for Bessel functions (of real and imaginary arguments, respectively), and $\bar{\alpha}_s=\alpha_s/3\pi$. The leading-order (LO) Glück-Reya-Vogt (GRV) set [53] was used in our calculations as the input collinear density.

Another set [54] is obtained from a unified BFKL and DGLAP description of F_2 data and includes the so called consistency constraint [55]. The consistency constraint introduces a large correction to the LO BFKL equation; about 70% of the full next to leading-order (NLO) corrections to the BFKL exponent λ are effectively included in this constraint, as is argued in [56].

The third set of gluon distribution functions is extracted from a numerical solution [57] of the CCFM equation [6].[1] Since the CCFM is an evolution equation in terms of the angle of the emitted partons, the corresponding gluon density $\mathcal{F}_g(x,k_T^2,\bar{q})$ differs from the other k_T-dependent gluon densities by the third argument $\bar{q}$, which is the scaled maximum emission angle. It may be argued [57] that the role of this variable is similar to that of μ^2 in the collinear gluon densities. Note, however, that the CCFM gluon splitting function contains only singular terms in the gluon momentum fraction z:

$$\mathcal{P}_{gg}(z)=\bar{\alpha}_s\left(\frac{1}{z}\Delta_{ns}+\frac{1}{1-z}\right), \tag{6}$$

with Δ_{ns} being the non-Sudakov form factor to regulate the $1/z$ singularity. The nonsingular terms of the splitting function are not included in the CCFM approximation [6]. On the other hand, the aforementioned approaches of Refs. [52] and [54] are based on the full DGLAP splitting function:

$$\mathcal{P}_{gg}(z)=\bar{\alpha}_s\left(\frac{1}{z}-2+z(1-z)+\frac{1}{1-z}\right). \tag{7}$$

The last, fourth approach was originally proposed in [1] and is now frequently discussed in the literature [8,58]. It recalls the kinematic relation between the virtuality q^2 and the transverse momentum k_T of a parton: $q^2=k_T^2/(1-x)$. Consequently, the ordinary (''integrated'') gluon distribution function $G(x,q^2)$ may be considered as giving the k_T^2 distribution also. In this approach, the unintegrated gluon density is derived from the ''integrated'' one by simply differentiating it with respect to q^2:

$$\mathcal{F}_g(x,k_T^2,\mu^2=k_T^2)=\frac{d}{dq^2}G(x,q^2)|_{q^2=k_T^2}. \tag{8}$$

III. DETAILS OF THE CALCULATION

Let k_1, k_2, k_3, p_c, and $p_{\bar{c}}$ be the momenta of the two incoming gluons, the outgoing gluon, and the outgoing heavy (charmed) quark and antiquark, respectively; $\epsilon_1,\epsilon_2,\epsilon_3$ the gluon polarization vectors; m_c the quark mass, $m_\psi=2m_c$, $k=k_1+k_2$, and a, b, c, and d the eightfold color indices of the two incoming gluons, the outgoing gluon, and the (colored) $c\bar{c}$ state. We also introduce the projection operator $J(S,L)$, which guarantees the proper spin and orbital angular momentum of the $c\bar{c}$ state under consideration. Then, the gluon-gluon fusion matrix elements read

$$\begin{aligned}\mathcal{M}_a(gg\to\psi g)=&\,\mathrm{tr}\{\not\epsilon_1(\not p_c-\not k_1+m_c)\not\epsilon_2\\&\times(-\not p_{\bar{c}}-\not k_3+m_c)\not\epsilon_3 J(S,L)\}C_\psi\\&\times\mathrm{tr}\{T^aT^bT^cT^d\}[k_1^2-2(p_ck_1)]^{-1}\\&\times[k_3^2+2(p_{\bar{c}}k_3)]^{-1}+5\ \text{permutations},\end{aligned} \tag{9}$$

$$\begin{aligned}\mathcal{M}_b(gg\to\psi g)=&\,\mathrm{tr}\{\gamma_\mu(\not p_c-\not k_3+m_c)\not\epsilon_3 J(S,L)\}\\&\times iG^{(3)}(k_1,\epsilon_1,k_2,\epsilon_2,-k,\mu)C_\psi f^{abe}\\&\times\mathrm{tr}\{T^eT^cT^d\}[k^2]^{-1}[k_3^2+2(p_{\bar{c}}k_3)]^{-1}\\&+5\ \text{permutations},\end{aligned} \tag{10}$$

$$\begin{aligned}\mathcal{M}_c(gg\to\psi g)=&\,\mathrm{tr}\{\gamma_\nu J(S,L)\}G^{(3)}(k_1,\epsilon_1,k_2,\epsilon_2,-k,\mu)\\&\times G^{(3)}(-k_3,\epsilon_3,-p_\psi,\epsilon_\psi,k,\nu)C_\psi f^{abe}f^{cfe}\\&\times\mathrm{tr}\{T^fT^d\}[k^2]^{-1}[m_\psi^2]^{-1}\\&+2\ \text{permutations},\end{aligned} \tag{11}$$

[1] A numerical parametrization of this set has been kindly offered by Hannes Jung in the form of a FORTRAN code.

$$\mathcal{M}_d(gg\to\psi g)=\mathrm{tr}\{\gamma_\nu J(S,L)\}G^{(4)A,B,C}(\epsilon_1,\epsilon_2,\epsilon_3,\nu)C_\psi \times \mathrm{tr}\{T^f T^d\}[m_\psi^2]^{-1}. \quad (12)$$

In the above expressions, $G^{(3)}$ and $G^{(4)}$ are related to the standard QCD three- and four-gluon couplings with $G^{(4)}$ being split into three terms with respect to their color structure:

$$G^{(3)}(p,\lambda,q,\mu,k,\nu)=[(q-p)^\nu g^{\lambda\mu}+(k-q)^\lambda g^{\mu\nu}+(p-k)^\mu g^{\nu\lambda}],$$

$$G^{(4)A}(\lambda,\mu,\nu,\sigma)=f^{abe}f^{cfe}(g^{\lambda\nu}g^{\mu\sigma}-g^{\lambda\sigma}g^{\mu\nu}),$$

$$G^{(4)B}(\lambda,\mu,\nu,\sigma)=f^{aef}f^{bce}(g^{\lambda\mu}g^{\nu\sigma}-g^{\lambda\sigma}g^{\mu\nu}),$$

$$G^{(4)C}(\lambda,\mu,\nu,\sigma)=f^{ace}f^{bef}(g^{\lambda\nu}g^{\mu\sigma}-g^{\lambda\mu}g^{\nu\sigma}).$$

The factor represented by the SU(3) generator matrix T^d has to be replaced by the unit matrix if the outgoing $c\bar{c}$ state is a color singlet. The coefficient C_ψ stands for the normalization of the $c\bar{c}$ color wave function and is equal to $1/\sqrt{3}$ and 1/2 for the singlet and octet states, respectively.

The projection operator $J(S,L)$ reads for the different spin and orbital angular momentum states [28,29]

$$J(^1S_0)\equiv J(S=0,L=0)=\gamma_5(\not{p}_c+m_c)/m_\psi^{1/2}, \quad (13)$$

$$J(^3S_1)\equiv J(S=1,L=0)=\not{\epsilon}(S_z)(\not{p}_c+m_c)/m_\psi^{1/2}, \quad (14)$$

$$J(^3P_J)\equiv J(S=1,L=1)=(\not{p}_{\bar{c}}-m_c)\not{\epsilon}(S_z)(\not{p}_c+m_c)/m_\psi^{3/2}. \quad (15)$$

States with various projections of the spin momentum onto the z axis are represented by the polarization vector $\epsilon(S_z)$.

In the nonrelativistic approximation which we are using, the relative momentum q of the quarks in the bound state is treated as a small quantity. So it is useful to represent the quark momenta as follows:

$$p_c=\frac{1}{2}p_\psi+q, \quad p_{\bar{c}}=\frac{1}{2}p_\psi-q, \quad (16)$$

where p_ψ is the momentum of the final state quarkonium. The probability for the two quarks to form a meson depends on the bound state wave function $\Psi(q)$. Therefore, we multiply the matrix elements (9)–(12) by $\Psi(q)$ and perform integration with respect to q. The integration is performed after expanding the integrand around $q=0$:

$$\mathcal{M}(q)=\mathcal{M}|_{q=0}+q^\alpha(\partial\mathcal{M}/\partial q^\alpha)|_{q=0}+\cdots. \quad (17)$$

Since the expressions for $\mathcal{M}|_{q=0}$, $(\partial\mathcal{M}/\partial q^\alpha)|_{q=0}$, etc., are no longer dependent on q, they may be factored outside the integral sign. A term-by-term integration of this series then yields [29]

$$\int\frac{d^3q}{(2\pi)^3}\Psi(q)=\frac{1}{\sqrt{4\pi}}\mathcal{R}(x=0), \quad (18)$$

$$\int\frac{d^3q}{(2\pi)^3}q^\alpha\Psi(q)=-i\epsilon^\alpha(L_z)\frac{\sqrt{3}}{\sqrt{4\pi}}\mathcal{R}'(x=0), \quad (19)$$

etc., where $\mathcal{R}(x)$ is the spatial component of the wave function in the coordinate representation [the Fourier transform of $\Psi(q)$]. The first term contributes only to S waves, but vanishes for P waves because $\mathcal{R}_P(0)=0$. On the contrary, the second term contributes only to P waves, but vanishes for S waves because $\mathcal{R}'_S(0)=0$. States with various projections of the orbital angular momentum onto the z axis are represented by the polarization vector $\epsilon(L_z)$.

The polarization vectors $\epsilon(S_z)$ and $\epsilon(L_z)$ are defined as explicit four-vectors. In the frame where the z axis is oriented along the quarkonium momentum vector, $p_\psi=(0,0,|p_\psi|,E_\psi)$, these polarization vectors read

$$\epsilon(\pm1)=(1,\pm i,0,0)/\sqrt{2}, \quad \epsilon(0)=(0,0,E_\psi,|p_\psi|)/m_\psi. \quad (20)$$

When necessary, states with definite S_z and L_z can be translated into states with definite total momentum J and its projection J_z using the Clebsch-Gordan coefficients:

$$\epsilon^{\mu\nu}(J,J_z)=\sum_{L_z,S_z}\langle 1,L_z;1,S_z|J,J_z\rangle\epsilon^\mu(L_z)\epsilon^\nu(S_z). \quad (21)$$

However, we do not use such a presentation in our calculations. We find it more convenient to operate directly with the polarization vectors $\epsilon(L_z)$ and $\epsilon(S_z)$ to properly include the interference [35] between color-octet states with different J.

As far as the gluon spin density matrix is concerned, we take for the off-shell incoming gluons [4]

$$\overline{\epsilon^\mu\epsilon^{*\nu}}=k_{iT}^\mu k_{iT}^\nu/|k_{iT}|^2. \quad (22)$$

The final state gluon in Eqs. (9)–(12) is assumed on shell, $\Sigma\epsilon_3^\mu\epsilon_3^{*\nu}=-g^{\mu\nu}$. The evaluation of the traces in Eqs. (9)–(12) is straightforward and is done using the algebraic manipulation system FORM [59].

It is worth saying that to observe gauge invariance with off-shell gluons is a problem, which can be solved by a rather artificial trick [4]. One starts with a set of "extended" diagrams, where the off-shell gluons are considered as emitted by exernal on-shell fields (say, quarks), and so are represented as internal lines in the Feynman graphs. As all of the external lines in these graphs are on shell, the gauge invariance of the whole set is not problematic. However, the full gauge invariant set may contain unfactorizable diagrams (different from those shown in Fig. 1), that is, diagrams that cannot be represented as a convolution of gluon-gluon fusion matrix elements with gluon distribution functions (for example, this extended set contains diagrams with gluon lines stretched between the two external quark lines; Figs. 5(e) and 5(d) in [4]). At the same time, we learn from Ref. [4] that the contribution from these unfactorizable graphs vanishes in the particular gauge (22), and so one is authorized to take into account only the usual graphs shown in Figs. 1(a)–1(d). We notice that in some exceptional cases, such as the production of J/ψ mesons via a direct color-singlet mechanism,

the diagrams shown in Fig. 1(a) are gauge invariant on their own, even with off-shell external gluons. In that case, the gauge invariance can be verified explicitly, by substituting the gluon momenta for their polarization vectors. This property also holds for the color-singlet production of χ_c states and for the color-octet subprocesses (29)–(31) mentioned below.

To calculate the cross section of a physical process we have to multiply the matrix elements squared by the gluon distribution functions and perform integration over the final state phase space. The multiparticle phase space $\Pi d^3p_i/(2E_i)\delta^4(\Sigma p_{in}-\Sigma p_{out})$ is parametrized in terms of transverse momenta, rapidities, and azimuthal angles: $d^3p_i/(2E_i)=(\pi/2)dp_{iT}^2dy_i d\phi_i/(2\pi)$. Let ϕ_1, ϕ_2, and ϕ_3 be the azimuthal angles of the initial and final gluons, and y_ψ and ϕ_ψ the rapidity and the azimuthal angle of the J/ψ particle. Then the fully differential cross section reads

$$d\sigma(pp\to\psi X)=\frac{4\pi^2\alpha_s^3|\mathcal{R}(0)|^2}{s^2}\frac{1}{4}\sum_{\text{spins}}\frac{1}{64}\sum_{\text{colors}}|\mathcal{M}(gg\to\psi g)|^2$$

$$\times\mathcal{F}_g(x_1,k_{1T}^2,\mu^2)\mathcal{F}_g(x_2,k_{2T}^2,\mu^2)dk_{1T}^2dk_{2T}^2dp_{\psi T}^2dy_3dy_\psi\frac{d\phi_1}{2\pi}\frac{d\phi_2}{2\pi}\frac{d\phi_\psi}{2\pi}. \tag{23}$$

The phase space physical boundary is determined by the inequality [60]

$$G(\hat{s},\hat{t},k_3^2,k_1^2,k_2^2,m_\psi^2)\leqslant 0, \tag{24}$$

where $\hat{s}=(k_1+k_2)^2$, $\hat{t}=(k_1-p_\psi)^2$, and G is the standard kinematic function [60].

The initial gluon momentum fractions x_1 and x_2 are calculated from the energy-momentum conservation laws in the light-cone projections:

$$(k_1+k_2)_{E+p_{||}}=x_1\sqrt{s}=m_{\psi T}\exp(y_\psi)+|k_{3T}|\exp(y_3),$$

$$(k_1+k_2)_{E-p_{||}}=x_2\sqrt{s}=m_{\psi T}\exp(-y_\psi)+|k_{3T}|\exp(-y_3), \tag{25}$$

$m_{\psi T}=(m_\psi^2+|p_{\psi T}|^2)^{1/2}$. Here, we preserve exact kinematics and do not neglect the ''small'' light-cone component of the gluon momentum. The multidimensional integration in Eq. (23) has been performed by means of the Monte Carlo technique, using the routine VEGAS [61]. The full FORTRAN code is available from the author on request.

IV. NUMERICAL RESULTS AND DISCUSSION

We begin the discussion by presenting a comparison between the predictions of the conventional and the k_T-factorization approaches for the J/ψ transverse momentum spectrum at Fermilab Tevatron conditions. For the collinear parton model, we use the gluon densities of Ref. [53]. In the k_T-factorization approach, we use the unintegrated distributions developed from the same GRV(LO) set in accordance with [52]. The renormalization scale in the strong coupling constant $\alpha_s(\mu^2)$ is chosen equal to the J/ψ transverse momentum in all cases, $\mu^2=p_{\psi T}^2$. The nonperturbative color-octet parameters are taken as in Ref. [33].

The solid and dashed histograms in Fig. 2 represent the color-singlet and $^3S_1[8]$ color-octet contributions in the collinear parton model. The difference in shape between these two contributions is due to the additional Feynman diagrams shown in Figs. 1(b)–1(d), whose p_T behavior is qualitatively different from that of Fig. 1(a). The production of J/ψ particles at high p_T is thought to be dominated by gluon fragmentation into the $^3S_1[8]$ state (dashed histogram) followed by a series of nonperturbative gluon emissions. The contributions from other octet states ($^1S_0[8]$ and $^3P_J[8]$, $J=0,1,2$) saturate the cross section at moderate p_T values (and are not shown in the figure). Although the agreement with the Tevatron data is apparently satisfactory, one should not forget the troubling issue of the photoproduction data and the problem of spin alignment.

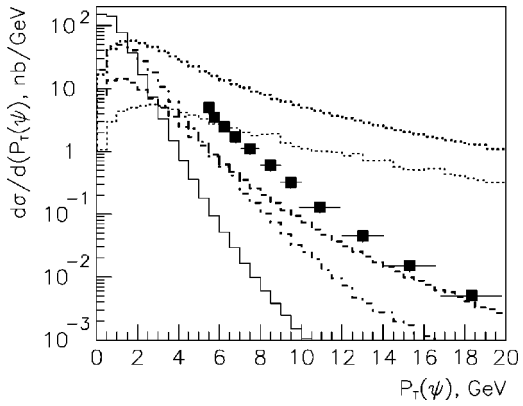

FIG. 2. J/ψ hadroproduction at Tevatron conditions $pp(\sqrt{s}=1.8$ TeV), $|\eta_\psi|\leqslant 0.6$: a comparison between the collinear and k_T-factorization approaches. Solid histogram, color-singlet contribution within the collinear approximation; dashed histogram, $^3S_1[8]$ color-octet contribution within the collinear approximation; dash-dotted histogram, color-singlet contribution within the k_T factorization; upper dotted histogram, color-octet contribution from the $2\to 1$ process (30) within the k_T factorization; lower dotted histogram, color-octet contribution from the $2\to 2$ process (27) within the k_T factorization, $q_{\text{reg}}^2=m_\psi^2$, $|\mathcal{R}_{^1S_0[8]}(0)|^2=8\times 10^{-3}$ GeV^3; ■, experimental data [24,25].

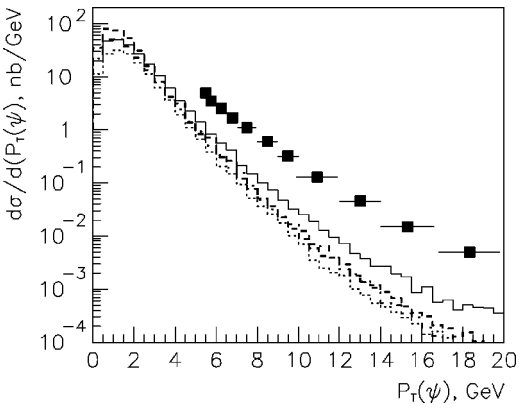

FIG. 3. The effect of the unintegrated gluon distribution functions on the size and shape of the color-singlet contribution: a comparison of four different parametrizations. Solid histogram, BFKL (Blümlein) [52]; dashed histogram, KMS [54]; dash-dotted histogram, CCFM [57]; dotted histogram, DGLAP; ■, experimental data [24,25].

An extension of the color-singlet model to the k_T-factorization approach shows a strong p_T broadening effect (dash-dotted histogram in Fig. 2), which is connected to the initial gluon transverse momentum. Although the absolute size of the production cross section does not change much, the enhancement of the differential cross section in the high p_T region brings the predictions of the color-singlet model into closer agreement with the data. A similar effect was considered earlier in Ref. [36] using calculations based on PYTHIA [62], and, also, in the k_T-factorization approach [19,50,51]. The authors came to the conclusion that, with the initial gluon transverse momentum taken into account, one needs some significantly lower values for the color-octet matrix elements to fit the Tevatron data. This, in turn, reduces the discrepancy between the theory and the electroproduction data where the color-octet contribution is not needed at all.

The size of the color-octet contribution, that is needed to fill the gap between the predictions of the color-singlet model and the hadroproduction data depends on the choice of the unintegrated gluon density. Figure 3 demonstrates the effect of using different parametrizations on the behavior of the color-singlet contribution. The curves obtained with BFKL, Kobo-Martin-Schwinger (KMS), CCFM, and DGLAP sets converge at $p_T \simeq 3$ GeV, but deviate from each other by about one order of magnitude at $p_T \simeq 20$ GeV. One can see that the formally subleading terms, such as the ones corresponding to the ''consistency constraint'' or the nonsingular parts of the gluon splitting function, introduce large differences in the predicted spectra.

Turning to the behavior of the color-octet contributions, we face another uncertainty, which is connected to the interplay between the $2\to2$ and $2\to1$ partonic subprocesses. In the collinear approximation, the perturbation expansion starts from the $2\to2$ subprocesses

$$g+g\to {}^1S_0[8]+g, \tag{26}$$

$$g+g\to {}^3S_1[8]+g, \tag{27}$$

$$g+g\to {}^3P_J[8]+g, \tag{28}$$

which are of order $O(\alpha_s^3)$. The formally lowest-order $2\to1$ subprocesses

$$g+g\to {}^1S_0[8], \tag{29}$$

$$g+g\to {}^3S_1[8], \tag{30}$$

$$g+g\to {}^3P_J[8] \tag{31}$$

do not contribute to the visible cross sections as they produce only states with zero p_T. On the contrary, in the k_T-factorization approach, the $2\to1$ subprocesses (29)–(31) are regarded as true leading order, while the $2\to2$ subprocesses (26)–(28) play the role of next-to-leading-order corrections.

When calculating the NLO contributions, one has to take care about the infrared instability of the relevant $2\to2$ matrix elements. In a rigorous approach, one has to consider the corresponding $2\to1$ subprocesses at next-to-leading order. Then, the interference between the LO and NLO contributions must cancel the infrared divergent parts of the $2\to2$ subprocesses. Such calculations have been performed in the collinear factorization in [63]. Since the corresponding results are not yet available in k_T factorization, we use an approximate phenomenological approach. In order to restrict the $2\to2$ subprocesses to the perturbative domain, we introduce the regularization parameter $q^2_{\rm reg}$, so that all propagators are kept away from their poles by a distance not less than $q^2_{\rm reg}$. It may be argued [30–32,64] that the nonperturbative parts of the $2\to2$ subprocesses can be absorbed into $2\to1$ subprocesses; that is, when the emitted gluon is soft, one can consider the final state as represented by a single particle rather than by two. In this approach, the regularization parameter $q^2_{\rm reg}$ in the $2\to2$ processes and the nonperturbative color-octet matrix elements in the $2\to1$ processes must be correlated [64] to avoid double counting between the hard and soft gluons in the final state (and so to avoid sensitivity of the results to the choice of $q^2_{\rm reg}$). If the regularization parameter is set to $q^2_{\rm reg}=1$ GeV^2 (that is, of order $\Lambda^2_{\rm QCD}$, which may be regarded as the lower limit of the perturbative domain), the contributions from the $2\to1$ and $2\to2$ subprocesses are quite comparable (see Fig. 4).

Given the regularization parameter and the color-octet matrix elements fixed at some arbitrary values, we display the behavior of the different partonic subprocesses in Fig. 5. The shapes of the curves representing ${}^1S_0[8]$ (dotted histograms) and ${}^3P_J[8]$ (dash-dotted histograms) color-octet channels are very similar to each other, both being very different from that of the ${}^3S_1[8]$ channel (dashed histograms). This feature is observed even in the $2\to1$ processes where the J/ψ transverse momentum is totally determined by the momenta of the initial gluons. Most likely, this property has to be attributed to the structure of the three-gluon coupling ($g^*+g^*\to g^*\to {}^3S_1[8]$), which cancels some powers of p_T^2 in the denominator. The difference in the p_T shapes between the different contributions that we see here agrees with the calculations made by other authors [50,51].

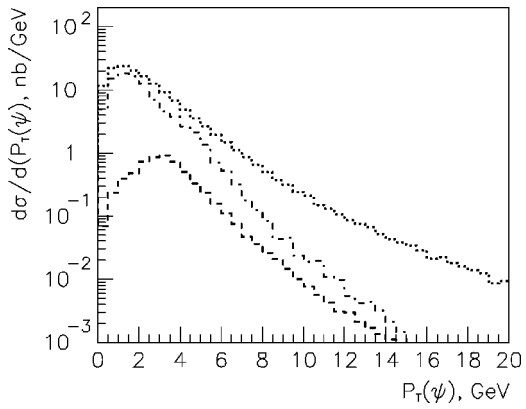

FIG. 4. The effect of the infrared cutoff on the size and the shape of color-octet contributions. Dotted histogram, contribution from subprocess (31); dashed histogram, contribution from subprocess (28) with $q^2_{\rm reg}=m^2_\psi$; dash-dotted histogram, contribution from subprocess (28) with $q^2_{\rm reg}=1$ GeV^2. The nonperturbative matrix element is kept fixed: $|\mathcal{R}'_{^3P_0[8]}(0)|^2=7\times10^{-3}$ GeV^5.

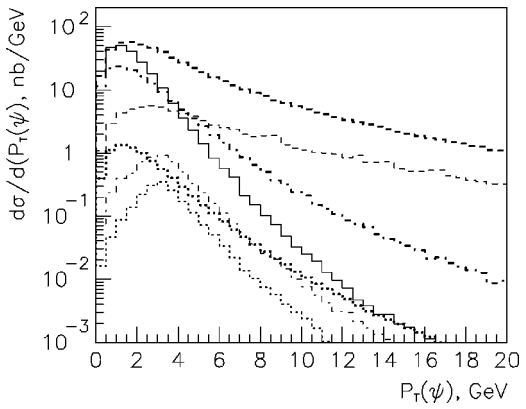

FIG. 5. Different color-octet and color-singlet contributions within the k_T-factorization approach. Solid histogram, color-singlet contribution; upper and lower dashed histograms, contributions from the subprocesses (30) and (27), respectively; upper and lower dash-dotted histograms, contributions from the subprocesses (31) and (28), respectively; upper and lower dotted histograms, contributions from the subprocesses (29) and (26), respectively. The parameter setting is as follows: $|\mathcal{R}_{^3S_1[1]}(0)|^2=8\times10^{-1}$ GeV^3, $|\mathcal{R}_{^1S_0[8]}(0)|^2=8\times10^{-3}$ GeV^3, $|\mathcal{R}_{^3S_1[8]}(0)|^2=8\times10^{-3}$ GeV^3, $|\mathcal{R}'_{^3P_0[8]}(0)|^2=7\times10^{-3}$ GeV^5, $q^2_{\rm reg}=m^2_\psi$.

As we have seen already in Fig. 2, the $^3S_1[8]$ channel shows an inadequate behavior of the p_T spectrum in comparison with the data. This means that the $^3S_1[8]$ channel cannot be the dominant one in the p_T region under study, and that the corresponding color-octet matrix element must be reduced by at least a factor of 50. The difference between the color-octet matrix elements, which we need to assign to fit the data, violates the nonrelativistic QCD (NRQCD) scaling rules.[2]

Before we proceed to the numerical fits, we find it useful to comment on the effect of the renormalization scale μ^2 in the strong coupling constant. The replacement $\alpha_s(p^2_{\psi T})^2 \to \alpha_s(k^2_{1T})\alpha_s(k^2_{2T})$ increases the predicted cross sections by a factor of 2.5 for the charmonium family, and by a factor of more than 3 for the bottomonium family.

We also recall that the shapes of all p_T distributions are sensitive to the choice of unintegrated gluon densities. Taken together, these uncertainties show that the theory cannot pretend to an accuracy better than a factor of 2 or 3 (which is also typical for the collinear calculations). In such a situation, we find it meaningless to invest effort in fine-tuning. The results shown in Figs. 6–8 are not intended to provide precise fits. They are only intended to demonstrate the qualitative behavior of the k_T-factorization approach and to show its qualitative compatibility with the data.

In Figs. 6, 7, and 8, we display the results for the production of J/ψ, χ_c, and Υ mesons at the Fermilab Tevatron, respectively. In general, our results for direct J/ψ production (Fig. 6) agree with the analysis of Ref. [50]. We observe only minor differences, which may be explained by the different choice of gluon distributions. In particular, we find that the data show no necessity for the presence of a $^3S_1[8]$ color-octet contribution. At least, the value of the corresponding nonperturbative matrix element needs to be reduced by a huge factor, compared to [33]. At the same time, the authors

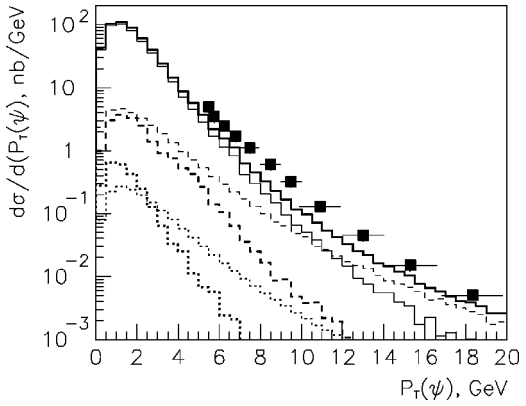

FIG. 6. The overall fit of the experimental data for J/ψ hadroproduction. The parameter settings are the BFKL gluon distribution function [52], $|\mathcal{R}_{^3S_1[1]}(0)|^2=8\times10^{-1}$ GeV^3, $|\mathcal{R}_{^1S_0[8]}(0)|^2=1.6\times10^{-3}$ GeV^3, $|\mathcal{R}_{^3S_1[8]}(0)|^2=0$, $|\mathcal{R}'_{^3P_0[8]}(0)|^2=1.4\times10^{-3}$ GeV^5, $q^2_{\rm reg}=1$ GeV^2. Thin solid histogram, color-singlet contribution; thick dashed histogram, contribution from subprocess (28); thin dashed histogram, contribution from subprocess (31); thick dotted histogram, contribution from subprocess (26); thin dotted histogram, contribution from subprocess (29); thick solid histogram, sum of all contributions; ■, experimental data [24,25].

[2]The authors of [51] point out the same inconsistency. According to their estimates, the difference between the $^1S_0[8]$ and $^3S_1[8]$ matrix elements amounts to a factor of 100. They suppose that "there might be some dynamical reasons [65]" or "there might be some new counting rules [66]" to account for the suppression of the $^3S_1[8]$ matrix elements. The authors of [50] estimate the difference between the values of $^3S_1[8]$ and M_8 (that is, a linear combination of $^1S_0[8]$ and $^3P_0[8]$) as a factor of 30, but they do not regard it as a kind of inconsistency.

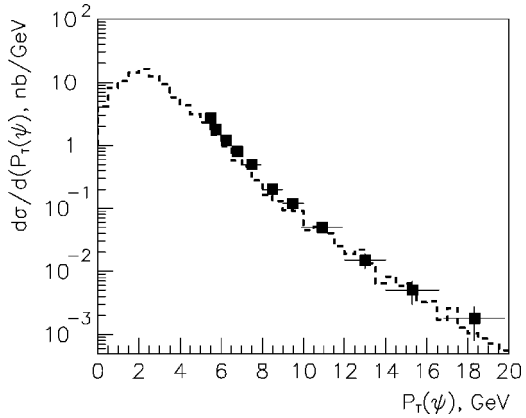

FIG. 7. The overall fit of the experimental data for the hadroproduction of J/ψmesons via $\chi_c$decays. Dashed histogram, color-singlet contribution with BFKL gluon distribution function [52] and $|\mathcal{R}'_{^3P_0[1]}(0)|^2=0.075$ GeV^5 [67]; ■, experimental data [24]–[26].

of [50] state that ''if this matrix element is put exactly to zero, the quality of the fit is much worse.''

Similarly, when we use the BFKL gluon density, we find no need for a color-octet contribution to the production of χ_c mesons (Fig. 7). At the same time, the calculations [20] using the KMS gluon density show that a small color-octet admixture improves the agreement with the data.

As far as the production of Υ is concerned (Fig. 8), one should keep in mind that the quoted data contain radiative feed-down from χ_b states, which brings about 51% [27] of the visible cross section. Therefore, to separate the direct production, the plotted data should be rescaled by an approximate factor of 1/2 (please note that the p_T dependence of these two contributions has not been measured separately). Once again, we observe the qualitative compatibility of the color-singlet contribution with the data.

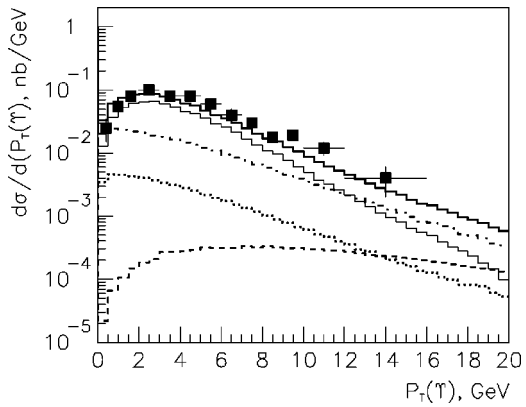

FIG. 8. The overall fit of the experimental data for the hadroproduction of Υ mesons at Tevatron conditions, $pp(\sqrt{s}=1.8$ TeV), $|\eta_\Upsilon|\leqslant 0.4$. The parameter settings are the BFKL gluon distribution function [52], $|\mathcal{R}_{^3S_1[1]}(0)|^2=6$ GeV^3, $|\mathcal{R}_{^1S_0[8]}(0)|^2=1\times10^{-1}$ GeV^3, $|\mathcal{R}_{^3S_1[8]}(0)|^2=6\times10^{-3}$ GeV^3, $|\mathcal{R}'_{^3P_0[8]}(0)|^2=0.5$ GeV^5, $q^2_{\rm reg}=10$ GeV^2. Thin solid histogram, color-singlet contribution; dotted histogram, contribution from $^1S_0[8]$ state; dashed histogram, contribution from $^3S_1[8]$ state; dash-dotted histogram, contribution from $^3P_J[8]$ states; thick solid histogram, sum of all contributions; ■, experimental data [24]–[27].

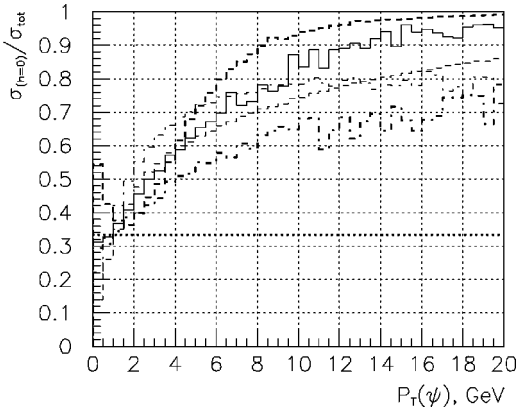

FIG. 9. The fraction of longitudinally polarized J/ψmesons as calculated for different particular contributions. Solid histogram, color-singlet contribution; thin and thick dashed histograms, contributions from subprocesses (30) and (27), respectively; thin and thick dash-dotted histograms, contributions from subprocesses (31) and (28), respectively; dotted histogram, contributions from subprocesses (29) and (26).

Now we turn to the most interesting part of the consideration. The clever idea [36] that, having taken the initial gluon transverse momentum into account, one needs lower values of the nonperturbative matrix elements to fit the Tevatron data, helps to overcome the apparent incompatibility between the electro- and hadroproduction model parameters. However, as long as the gluon off-shellness is ignored, the problem of J/ψ spin alignment remains unsolved. It is instructive to analyze the effects of gluon off-shellness on the J/ψ polarization properties within the k_T-factorization approach.

We are arriving at the key point of the present paper. Figure 9 shows the results of our calculations regarding the different contributing mechanisms. Remarkably, the fraction of longitudinally polarized mesons increases with p_T in all cases, including both color-singlet and color-octet contributions. The only exception refers to the $^1S_0[8]$ state, which is produced unpolarized because of its spinless nature. The property of large longitudinal polarization holds even for the $^3S_1[8]$ state, although its production at large p_T is believed to be dominated by the gluon fragmentation.[3]

As a matter of academic interest, we have checked that the longitudinal polarization strengthens continuously with increasing p_T, and, consequently, the k_T-factorization approach does not merge with the ''collinear'' interpretation of

[3]Our result is in contradiction with the analysis of Yuan and Chao [51], which also relies on the k_T-factorization approach. Unfortunately, the authors provide too few details on their method of calculation to disclose the origin of the discrepancy. In particular, they do not specify the off-shell gluon spin density matrix and do not present the definition of J/ψ helicity states. One can find some more details in their previous paper [19], which is devoted to the production of color-singlet states (also in the k_T-factorization scheme). However, even there, the explanations are insufficient.

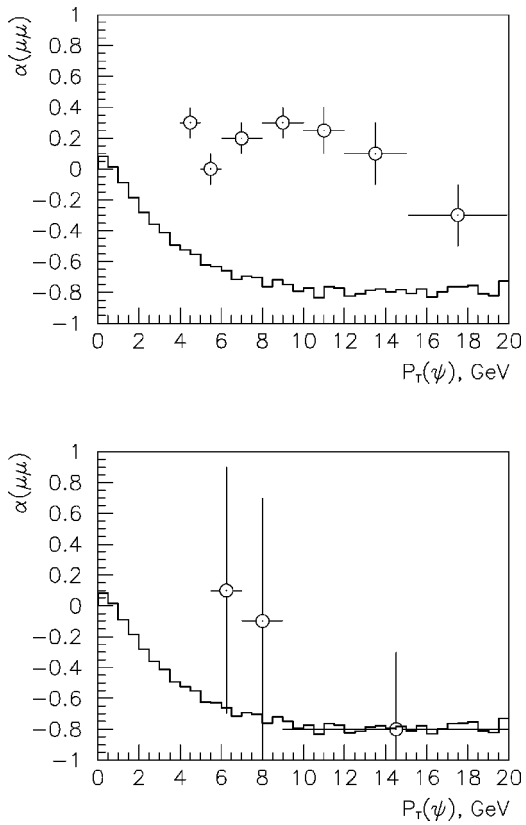

FIG. 10. Model predictions for the J/ψ(upper panel) and ψ' (lower panel) spin alignment at Tevatron conditions. The parameter setting is as in Fig. 6; ⊙, experimental data [49].

QCD in the high p_T limit. Although the validity of the k_T factorization at high p_T may be doubted, it may provide an improved treatment of the moderate p_T region in comparison with the collinear factorization, where the contribution from longitudinally polarized gluons is neglected. As the data taken into analysis are restricted to $p_T<20$ GeV, which is a small quantity compared to $\sqrt{s}=1.8$ TeV, the applicability of the k_T factorization is justified.

A comparison with the available data on the charmonium spin alignment shows that nature tends to favor the k_T-factorization approach. The polarization of ψ' mesons provides a cleaner sample than the polarization of J/ψ mesons since the former is not contaminated by feed-down from χ_c decays. The preliminary results obtained by the Collider Detector at Fermilab (CDF) Collaboration [49] are displayed in Fig. 10 together with the theoretical estimations expressed in terms of the leptonic decay angular parameter α, which characterizes the azimuthal angle asymmetry measured in the J/ψ rest frame with respect to a given reference axis: $d\Gamma_{ll}/d\cos\Theta \sim 1+\alpha\cos^2\Theta$. At the Tevatron conditions, the reference axis is connected to the laboratory system (the same as the pp c.m. system). The cases $\alpha=1$ and $\alpha=-1$ correspond to transverse and longitudinal polarization of the J/ψ meson, respectively. We emphasize that the data not only point to unpolarized ψ' production at moderate p_T, but also to essentially longitudinal polarization at higher p_T. This feature is perfectly accommodated in our calculations.

The predictions made for the J/ψ photoproduction at HERA possess the same kind of behavior. A comparison with recent experimental data collected by the collaborations ZEUS [22] and H1 [23] is presented in Figs. 11 and 12, respectively. In both cases, the polarization analysis is performed in the so called target frame, that is, the rest system of the J/ψ meson, using the direction opposite to that of the incoming proton as reference axis. Although the experimental errors are rather large, the data seem to support the trend observed in the k_T-factorization approach. However, the data still preclude any definitive conclusions on the favorable set of unintegrated gluon densities. The theoretical results shown here have been confirmed by an independent calculation in [68].

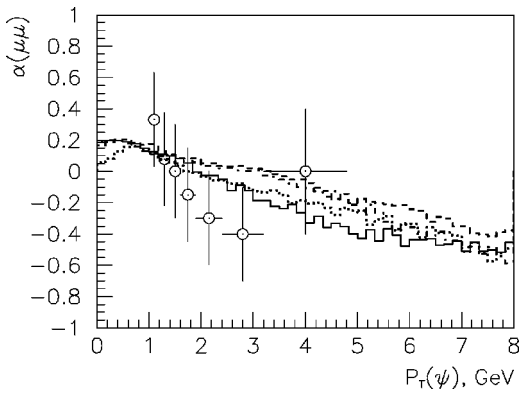

FIG. 11. Model predictions for the J/ψ spin alignment at the HERA ZEUS conditions, $ep(\sqrt{s}=300$ GeV), $Q^2<1$ GeV^2, 50 GeV $<W<180$ GeV, $0.4<z_\psi<1.0$. A comparison of different gluon distributions: Solid histogram, BFKL (Blümlein) [52]; dashed histogram, KMS [54]; dash-dotted histogram, CCFM [57]; dotted histogram, DGLAP; ⊙, experimental data [22].

In conclusion, we point out that the qualitative predictions for the J/ψ polarization are stable with respect to variations in the model parameters. In fact, there is no dependence on the α_s constant (which cancels out), and there is only weak sensitivity to the inclusion of next-to-leading-order subpro-

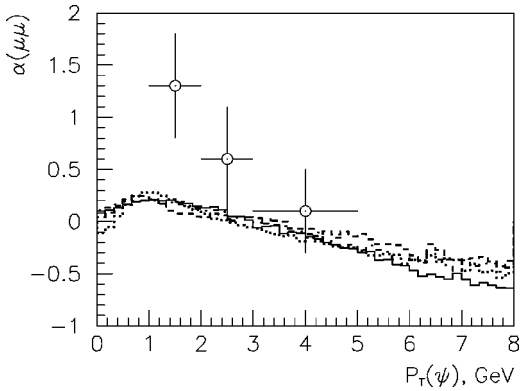

FIG. 12. Model predictions for the J/ψ spin alignment at HERA H1 conditions, $ep(\sqrt{s}=300$ GeV), $Q^2<1$ GeV^2, 60 GeV $<W<260$ GeV, $0.05<z_\psi<0.9$. A comparison of different gluon distributions: Solid histogram, BFKL (Blümlein) [52]; dashed histogram, KMS [54]; dash-dotted histogram, CCFM [57]; dotted histogram, DGLAP; ⊙, experimental data [23].

cesses and to the values of the color-octet matrix elements because the behavior of all contributions is very similar.

V. CONCLUSIONS

Here we have addressed the issue of performing a global analysis of quarkonium production within the k_T-factorization approach. The state of the art has not yet reached the precise quantitative level, and the theoretical predictions remain rather qualitative than quantitative. There are significant uncertainties connected with the choice of the unintegrated gluon densities, the renormalization scale in the strong coupling constant, the inclusion of next-to-leading-order subprocesses, and the nonperturbative color-octet transitions. At the moment, it seems impossible to unambiguously fix all the relevant parameters by adjusting them to the available experimental data.

At the same time, the k_T-factorization approach shows a number of important achievements. As a general feature, the model behavior is found to be perfectly compatible with the available data on the production of various quarkonium states at modern colliders. The model succeeds in describing the p_T spectra of J/ψ, χ_c, and Υ mesons at the Fermilab Tevatron and provides a consistent picture of the production of J/ψ mesons in deep inelastic scattering at HERA. The model even succeeds in describing the polarization phenomena observed in both pp and ep interactions, thus providing an important insight for solving a long-term puzzle.

The underlying physics is essentially related to the initial gluon off-shellness, which dominates the gluon polarization properties and has a considerable impact on the kinematics. On the experimental side, we note the fundamental role of the polarization variables, which make the difference between the collinear and noncollinear approaches clearly visible.

ACKNOWLEDGMENTS

The author conveys his thanks to Leif Jönsson, Hannes Jung, and especially Nikolai Zotov for their encouraging interest and useful discussions. The work was supported by the Royal Swedish Academy of Sciences.

[1] L. V. Gribov, E. M. Levin, and M. G. Ryskin, Phys. Rep. **100**, 1 (1983).
[2] E. M. Levin and M. G. Ryskin, Phys. Rep. **189**, 267 (1990).
[3] S. Catani, M. Ciafaloni, and F. Hautmann, Phys. Lett. B **242**, 97 (1990); Nucl. Phys. **B366**, 135 (1991).
[4] J. C. Collins and R. K. Ellis, Nucl. Phys. **B360**, 3 (1991).
[5] E. A. Kuraev, L. N. Lipatov, and V. S. Fadin, Sov. Phys. JETP **45**, 199 (1977); Ya. Balitskiĭ and L. N. Lipatov, Sov. J. Nucl. Phys. **28**, 822 (1978).
[6] M. Ciafaloni, Nucl. Phys. **B296**, 49 (1998); S. Catani, F. Fiorani, and G. Marchesini, Phys. Lett. B **234**, 339 (1990); Nucl. Phys. **B336**, 18 (1990); G. Marchesini, *ibid.* **B445**, 49 (1995).
[7] V. N. Gribov and L. N. Lipatov, Sov. J. Nucl. Phys. **15**, 438 (1972); G. Altarelli and G. Parisi, Nucl. Phys. **B126**, 298 (1977); Yu. L. Dokshitzer, Sov. Phys. JETP **46**, 641 (1977).
[8] E. M. Levin, M. G. Ryskin, Yu. M. Shabelski, and A. G. Shuvaev, Sov. J. Nucl. Phys. **53**, 1059 (1991); **54**, 1420 (1991); M. G. Ryskin, Yu. M. Shabelski, and A. G. Shuvaev, Z. Phys. C **69**, 269 (1996).
[9] J. R. Forshaw and R. G. Roberts, Phys. Lett. B **335**, 494 (1994).
[10] V. Del Duca, Sci. Acta **10**, 91 (1995).
[11] V. A. Saleev and N. P. Zotov, Mod. Phys. Lett. A **9**, 151 (1994); **11**, 25 (1996).
[12] A. V. Lipatov and N. P. Zotov, Mod. Phys. Lett. A **15**, 695 (2000); A. V. Lipatov, V. A. Saleev, and N. P. Zotov, *ibid.* **15**, 1727 (2000).
[13] S. P. Baranov and N. P. Zotov, Phys. Lett. B **458**, 389 (1999).
[14] S. P. Baranov, H. Jung, and N. P. Zotov, Nucl. Phys. (Proc. Suppl.) **B99**, 192 (2000).
[15] H. Jung, in *Proceedings of the Workshop on Monte Carlo Generators*, edited by A. Doyle, G. Grindhammer, G. Ingelman, and H. Jung (DESY, Hamburg, 1999), p. 75.
[16] S. P. Baranov and N. P. Zotov, Phys. Lett. B **491**, 111 (2000).
[17] S. P. Baranov and M. Smižanská, Phys. Rev. D **62**, 014012 (2000).
[18] Ph. Hägler, R. Kirschner, A. Shäfer, L. Szymanowski, and O. V. Teryaev, Phys. Rev. D **62**, 071502 (2000).
[19] F. Yuan and K.-T. Chao, Phys. Rev. D **63**, 034006 (2001).
[20] Ph. Hägler, R. Kirschner, A. Shäfer, L. Szymanowski, and O. V. Teryaev, Phys. Rev. Lett. **86**, 1446 (2001).
[21] S. P. Baranov, Phys. Lett. B **428**, 377 (1998).
[22] R. Brugnera, in *Deep Inelastic Scattering*, Proceedings of the Ninth International Workshop, Bologna, Italy, 2001, edited by G. Bruni, G. Iacobucci, and R. Nania (World Scientific, Singapore, 2002).
[23] H1 Collaboration, C. Adloff *et al.*, Eur. Phys. J. C **25**, 25 (2002).
[24] CDF Collaboration, V. Papadimitriou, Report No. FERMILAB Conf-95/128-E, 1995; A. Sansoni, Report No. FERMILAB Conf-95/263-E, 1995; K. Ohl, Report No. FERMILAB Conf-96/110-E, 1996; R. Demina, Report No. FERMILAB Conf-96/201-E, 1996; M. Bailey, Report No. FERMILAB Conf-96/235-E, 1996.
[25] CDF Collaboration, F. Abe *et al.*, Phys. Rev. Lett. **69**, 3704 (1992); **71**, 2537 (1993); **75**, 1451 (1995); **79**, 578 (1997).
[26] CDF Collaboration, T. Affolder *et al.*, Phys. Rev. Lett. **86**, 3963 (2001).
[27] CDF Collaboration, T. Affolder *et al.*, Phys. Rev. Lett. **84**, 2094 (2000).
[28] C.-H. Chang, Nucl. Phys. **B172**, 425 (1980); R. Baier and R. Rückl, Phys. Lett. B **102**, 364 (1981); E. L. Berger and D. Jones, Phys. Rev. D **23**, 1521 (1981).
[29] H. Krasemann, Z. Phys. C **1**, 189 (1979); G. Guberina, J. Kühn, R. Peccei, and R. Rückl, Nucl. Phys. **B174**, 317 (1980).
[30] E. Braaten and S. Fleming, Phys. Rev. Lett. **74**, 3327 (1995).
[31] M. Cacciari, M. Greco, M. L. Mangano, and A. Petrelli, Phys. Lett. B **356**, 560 (1995).
[32] G. T. Bodwin, E. Braaten, and G. P. Lepage, Phys. Rev. D **51**,

1125 (1995); **55**, 5855(E) (1997).
[33] P. Cho and A. K. Leibovich, Phys. Rev. D **53**, 150 (1996); **53**, 6203 (1996).
[34] W. K. Tang and M. Vänttinen, Phys. Rev. D **53**, 4851 (1996); **54**, 4349 (1996).
[35] E. Braaten and Y.-Q. Chen, Phys. Rev. D **54**, 3216 (1996).
[36] B. Cano-Coloma and M.-A. Sanchis-Lozano, Phys. Lett. B **406**, 232 (1997); Nucl. Phys. **B508**, 753 (1997).
[37] B. A. Kniehl and G. Kramer, Eur. Phys. J. C **6**, 493 (1999).
[38] K. Sridhar, A. D. Martin, and W. J. Stirling, Phys. Lett. B **438**, 211 (1998).
[39] H1 Collaboration, S. Aid *et al.*, Nucl. Phys. **B468**, 3 (1996); **B472**, 3 (1996).
[40] ZEUS Collaboration, J. Breitweg *et al.*, Z. Phys. C **76**, 599 (1997).
[41] M. Cacciari and M. Krämer, Phys. Rev. Lett. **76**, 4128 (1996).
[42] P. Ko, J. Lee, and H.-S. Song, Phys. Rev. D **54**, 4312 (1996).
[43] M. Beneke, M. Krämer, and M. Vänttinen, Phys. Rev. D **57**, 4258 (1998).
[44] M. Krämer, Nucl. Phys. **B459**, 3 (1996).
[45] M. Beneke and M. Krämer, Phys. Rev. D **55**, 5269 (1997).
[46] A. K. Leibovich, Phys. Rev. D **56**, 4412 (1997).
[47] E. Braaten, B. Kniehl, and J. Lee, Phys. Rev. D **62**, 094005 (2000).
[48] E537 Collaboration, C. Akerlof *et al.*, Phys. Rev. D **48**, 5067 (1993).
[49] CDF Collaboration, T. Affolder *et al.*, Phys. Rev. Lett. **85**, 2886 (2000).
[50] Ph. Hägler, R. Kirschner, A. Shäfer, L. Szymanowski, and O. V. Teryaev, Phys. Rev. D **63**, 077501 (2001).
[51] F. Yuan and K.-T. Chao, Phys. Rev. Lett. **87**, 022002 (2001).
[52] J. Blümlein, Report No. DESY 95-121, 1995.
[53] M. Glück, E. Reya, and A. Vogt, Z. Phys. C **67**, 433 (1995).
[54] J. Kwiecinski, A. Martin, and A. Stasto, Phys. Rev. D **56**, 3991 (1997).
[55] J. Kwiecinski, A. Martin, and A. Sutton, Phys. Rev. D **52**, 1445 (1995); Z. Phys. C **71**, 585 (1996).
[56] J. Kwiecinski, A. Martin, and J. Outhwaite, Eur. Phys. J. C **9**, 611 (2001).
[57] H. Jung and G. Salam, Eur. Phys. J. C **19**, 351 (2001).
[58] N. Nikolaev and B. Zakharov, Nucl. Phys. **B333**, 250 (1994).
[59] J. A. M. Vermaseren, *Symbolic Manipulations with FORM* (Computer Algebra Nederland, Amsterdam, 1991).
[60] E. Bycling and K. Kajantie, *Particle Kinematics* (John Wiley and Sons, New York, 1973).
[61] G. P. Lepage, J. Comput. Phys. **27**, 192 (1978).
[62] T. Sjöstrand, Comput. Phys. Commun. **82**, 74 (1994).
[63] A. Petrelli, M. Cacciari, M. Greco, F. Maltoni, and M. L. Mangano, Nucl. Phys. **B514**, 245 (1998).
[64] S. P. Baranov, Nucl. Phys. B (Proc. Suppl.) **93**, 226 (2001).
[65] C. Y. Wong, Phys. Rev. D **60**, 114025 (1999).
[66] S. Fleming, A. Leibovich, and I. Rothstein, Phys. Rev. D **64**, 036002 (2001).
[67] E. J. Eichten and C. Quigg, Phys. Rev. D **52**, 1726 (1995).
[68] V. A. Saleev, Phys. Rev. D **65**, 054041 (2002).